AGU PUBLICATIONS

JGR

Journal of Geophysical Research: Space Physics

RESEARCH ARTICLE
10.1002/2017JA024611

SC-Associated Electric Field Variations in the Magnetosphere and Ionospheric Convective Flows

S.-I. Kim[1], K.-H. Kim[1], H.-J. Kwon[2], H. Jin[1], E. Lee[1], G. Jee[2], N. Nishitani[3], T. Hori[3], M. Lester[4], and J. R. Wygant[5]

[1]School of Space Research, Kyung Hee University, Yongin, South Korea, [2]Division of Climate Change Research, Korea Polar Research Institute, Incheon, South Korea, [3]Institute for Space-Earth Environmental Research, Nagoya University, Nagoya, Japan, [4]Physics and Astronomy, University of Leicester, Leicester, UK, [5]Department of Physics and Astronomy, University of Minnesota, Twin Cities, Minneapolis, MN, USA

Key Points:
- SC-associated *E* field signature changes with local time during SC interval
- The *E* field variation is associated with magnetospheric convection flow enhanced during SC interval
- Ionospheric convection flow is strongly connected with SC-associated *E* field variation

Correspondence to:
K.-H. Kim,
khan@khu.ac.kr

Citation:
Kim, S.-I., Kim, K.-H., Kwon, H.-J., Jin, H., Lee, E., Jee, G., … Wygant, J. (2017). SC-associated electric field variations in the magnetosphere and ionospheric convective flows. *Journal of Geophysical Research: Space Physics*, *122*, 11,044–11,057. https://doi.org/10.1002/2017JA024611

Received 21 JUL 2017
Accepted 1 OCT 2017
Accepted article online 9 OCT 2017
Published online 6 NOV 2017

Abstract We examine magnetic and electric field perturbations associated with a sudden commencement (SC), caused by an interplanetary (IP) shock passing over the Earth's magnetosphere on 16 February 2013. The SC was identified in the magnetic and electric field data measured at Time History of Events and Macroscale Interactions during Substorms (THEMIS-E; THE-E: magnetic local time (MLT) = 12.4, L = 6.3), Van Allen Probe-A (VAP-A: MLT = 3.2, L = 5.1), and Van Allen Probe-B (VAP-B: MLT = 0.2. L = 4.9) in the magnetosphere. During the SC interval, THE-E observed a dawnward-then-duskward electric (*E*) field perturbation around noon, while VAP-B observed a duskward *E* field perturbation around midnight. VAP-A observed a dawnward-then-duskward *E* field perturbation in the postmidnight sector, but the duration and magnitude of the dawnward *E* perturbation are much shorter and weaker than that at THE-E. That is, the *E* field signature changes with local time during the SC interval. The Super Dual Auroral Radar Network radar data indicate that the ionospheric plasma motions during the SC are mainly due to the *E* field variations observed in space. This indicates that the SC-associated *E* field in space plays a significant role in determining the dynamic variations of the ionospheric convection flow. By comparing previous SC MHD simulations and our observations, we suggest that the *E* field variations observed at the spacecraft are produced by magnetospheric convection flows due to deformation of the magnetosphere as the IP shock sweeps the magnetopause.

1. Introduction

Transient ground magnetic field signatures responding to an interplanetary (IP) shock are referred to as a geomagnetic sudden commencement (SC) (see Araki, 1994, and references therein). At low and middle latitudes on the ground, the SC signatures exhibit a simple step-like increase in the horizontal (*H*) component. At high latitudes, however, they show a bipolar magnetic field variation consisting of two pulses with opposite polarities in the *H* component. The former variation is called a preliminary impulse (PI), and the latter is called a main impulse (MI). Since a bipolar signature occurs for a stepwise increase in the solar wind dynamic pressure, it cannot be explained by changes in the magnetopause current (i.e., inward magnetopause motions), which produces low-latitude magnetic field perturbations (e.g., Kim et al., 2002, 2004; Russell et al., 1992), associated with changes in the solar wind dynamic pressure. In order to explain why the ground SC signatures vary with latitudes, Araki (1994) developed a qualitative model for ground SCs using the current system combined with magnetopause currents, field-aligned currents (FACs), and ionospheric currents.

In the SC model, it has been suggested that PI-associated FACs (PI-FACs) are caused by the coupling of the fast mode waves, which are launched at the magnetopause when the magnetosphere is suddenly compressed by an IP shock, to shear Alfvén waves contributing to FACs due to the radial inhomogeneity in the magnetosphere (Chen & Hasegawa, 1974; Southwood, 1974; Tamao, 1965). Thus, the magnetospheric convection flows are not directly connected with ionospheric convection flows during the PI phase. The PI-associated FACs flow into the dusk ionosphere and out of the dawn ionosphere, producing a twin vortex current system with a counterclockwise Hall current vortex on the morning side and a clockwise Hall current vortex on the afternoon side in the ionosphere. The MI perturbation is associated with FACs, which are opposite direction to PI-FACs, produced by a duskward electric field connected to a newly enhanced magnetospheric convection in the new

compressed state of the magnetosphere after the passage of the fast mode wave front propagating tailward. The MI-associated FACs (MI-FACs) flowing into the dawn ionosphere and out of the dusk ionosphere also generate a twin vortex Hall ionospheric current with opposite sense to the PI-associated twin vortex current system. It has been known that these Hall currents produce the ground magnetic field perturbations for the PI phase and MI phase.

Following the work of Araki (1994), a number of numerical studies have been performed to explain the ground SC signatures (e.g., Fujita, Tanaka, Kikuchi, Fujimoto, Hosokawa, et al., 2003; Fujita, Tanaka, Kikuchi, Fujimoto, et al., 2003; Kim et al., 2009; Yu & Ridley, 2009; Samsonov et al., 2010; Slinker et al., 1999; Sun et al., 2015). These studies emphasized the importance of coupling between the magnetosphere and ionosphere via FACs and showed that the FACs responsible for the MI phase are associated with vortical plasma motions in the outer magnetosphere. For PI-FACs, Fujita, Tanaka, Kikuchi, Fujimoto, Hosokawa, et al. (2003) found that an enhanced dawn-to-dusk magnetopause current turns to the magnetosphere along the fast mode compressional wave front propagating to later local times in the outer magnetosphere, and this cross-field current in the magnetosphere is converted to a FAC through mode coupling when the compressional wave passes the coupling region of the steep Alfvén velocity gradient. Since such a region is located just outside the plasmapause located around $L = 4–5$, Fujita, Tanaka, Kikuchi, Fujimoto, Hosokawa, et al. (2003) used an unrealistic Alfvén speed profile in which the Alfvén speed is enhanced in a region of $L = 6–7$ to explain the PI signatures at higher latitudes (>70° magnetic latitude (MLAT)), corresponding to $L > 8$. According to a numerical study by Yu and Ridley (2009), PI-FACs can be produced by dusk-to-dawn electric fields, which cause a dusk-to-dawn displacement current, inside the magnetopause, launched by a fast mode. The authors assumed a monotonic radial Alfvén speed profile (i.e., they did not incorporate the plasmasphere) in their simulation. Thus, the position where the displacement current turns into a FAC is not a region of a significant Alfvén speed gradient, implying that mode coupling is not a main factor for PI-FACs.

Satellite observations at geosynchronous orbit show a strong local time asymmetry of SC amplitudes with a maximum amplitude near noon and a minimum amplitude near midnight (e.g., Borodkova et al., 2005; Kokubun, 1983; Kuwashima et al., 1985; Park et al., 2012; Villante & Piersanti, 2008; Wang et al., 2009). Such a day-night asymmetry of geosynchronous SC amplitudes may be due to the fact that SC-associated magnetopause and tail currents mainly contribute to geosynchronous magnetic field perturbations on the dayside and nightside, respectively. It has been reported that the propagation speed of SC-associated magnetic field perturbations in the magnetosphere is comparable to the fast mode speed, which is usually greater than the propagation speed of an IP shock in the solar wind (e.g., Baumjohann et al., 1983; Keika et al., 2009; Knott et al., 1985; Nopper et al., 1982; Sugiura et al., 1968; Wilken et al., 1982). However, there are previous studies reporting that the propagation speed of SC is much slower than the fast mode speed in the magnetotail (Huttunen et al., 2005; Kawano et al., 1992; Kim et al., 2004). The authors suggested that the major field change of SC in the magnetotail is due to lateral increases in the solar wind dynamic pressure squeezing the magnetotail and moving tailward.

The response of the magnetospheric plasma to solar wind pressure variations producing SC has been discussed using electric field and plasma data obtained in the magnetosphere. Baumjohann et al. (1983) observed magnetospheric plasma drifts rotating toward dusk from an antisunward direction, corresponding to a clockwise flow vortex, at geosynchronous orbit in the morning sector during traversal of an IP shock. Similar SC-associated plasma convection flows, estimated from electric and magnetic field data, near geosynchronous orbit in the morning sector have been reported by Kim et al. (2012). Most recently, Tian et al. (2016) used ion bulk velocity data in the outer magnetosphere of the prenoon sector during an SC interval and observed a clockwise flow vortex. Since the vortical flows reported in the previous studies appear a few minutes after the SC onset, it has been suggested that the MI-FACs are correlated with the vortical flow motions (e.g., Fujita, Tanaka, Kikuchi, Fujimoto, et al., 2003; Kim et al., 2009).

Shinbori et al. (2004) statistically examined the initial electric field perturbations of SCs corresponding to the interval of the PI phase in the inner magnetosphere ($L < 4$) and observed that the initial excursion of the electric field tends to be directed westward without local time dependence. The authors showed that the Poynting vector of the initial SC impulse is directed earthward for all local times. On the dayside, the initial westward electric field perturbations of SCs can be interpreted as the fast mode waves propagating tailward. On the nightside, however, it should be examined whether the initial perturbations of SCs are associated with fast mode waves propagating earthward, which is opposite to the direction on the dayside, because the westward

Table 1
Locations of IMAGE Stations

		Geographic		AACGM	
Site name	Site code	Latitude	Longitude	Latitude	Longitude
Longyearbyen	LYR	78.20°N	15.82°E	75.54°N	109.59°E
Homsund	HOR	77.00°N	15.60°E	74.40°N	107.36°E
Bear Island	BJN	74.50°N	19.20°E	71.74°N	106.57°E
Soroya	SOR	70.54°N	22.22°E	67.63°N	105.13°E
Lycksele	LYC	64.61°N	18.75°E	61.67°N	98.58°E

electric perturbation on the nightside can be generated by the earthward convection flow associated with SC (e.g., Kim et al., 2009; Samsonov and Sibeck, 2013; Shi et al., 2014; Sun et al., 2015).

In this study, we present a detailed analysis of the relationship between the electric field perturbations and ionospheric convection flows of an SC event observed on 16 February (Day 47) 2013. Although numerous SC studies have been conducted using magnetic and electric field data in space and magnetic field data on the ground, there is no direct comparison between the SC-associated *E* field variations and ionospheric convection flows from multipoint observations in the magnetosphere and ionosphere. Using the electric and magnetic field data obtained in space and the SuperDARN radar data obtained in the iosnosphere, we show that the ionospheric convection flows at high and middle latitudes are strongly connected with the SC-associated electric field variations observed in space for the PI and MI phases. We discuss whether these observations can be explained by the qualitative SC model (Araki, 1994) by comparing them with previous numerical studies. We note that the term "SC" is used for a sudden *H* component increase at low latitudes if a geomagnetic storm follows and the term "sudden impulse (SI)" is used without a following magnetic storm. Since SI has been proved to be caused by the same mechanism as SC, we use the term "SC" instead of "SI" in this study even though a magnetic storm follows our event.

The organization of the paper is as follows. Section 2 describes the satellite and ground experiments. Section 3 describes the data analysis. Section 4 presents a discussion, and section 5 concludes the study.

2. Data Sets

We use the solar wind and IMF data from the Solar Wind Experiment (SWE) (Ogilvie et al., 1995) and Magnetic Fields Investigation (MFI) (Lepping et al., 1995) instruments, respectively, on the Wind spacecraft to identify the IP shock in the solar wind on 16 February 2013. The magnetic (Auster et al., 2008) and electric field (Bonnell et al., 2008) data obtained from Time History of Events and Macroscale Interactions during Substorms (THEMIS-E; THE-E) around noon at $L = 6.3$ are used to examine dayside magnetospheric responses to the IP shock. We also use the magnetic (Kletzing et al., 2013) and electric field (Wygant et al., 2013) data obtained from the Van Allen Probe-A (VAP-A) in the postmidnight sector at $L = 5.1$ and Van Allen Probe-B (VAP-B) around midnight at $L = 4.9$ for nightside magnetospheric responses to the shock.

We use the 1 min *SYM-H* index (Iyemori & Rao, 1996) to identify the SC event at middle/low latitudes on the ground. For SC observations at high latitudes on the ground, we use geomagnetic field data from the IMAGE (International Monitor for Auroral Geomagnetic Effects) stations (Lühr, 1994). Table 1 lists the five stations selected from the IMAGE ground magnetometer network. The magnetic coordinates listed in the table are defined in the Altitude Adjusted Corrected Geomagnetic Coordinates (AACGM) system (Shepherd, 2014) and calculated for the year 2013 (altitude 100 km) by using the online service provided at http://sdnet.thayer.dartmouth.edu/aacgm/aacgm_calc.php#AACGM. To examine the ionospheric response to the IP shock, we use the SuperDARN Pykkvibaer (PYK, geographic coordinates: 63.86°N, 19.20°W) radar (Ruohoniemi & Baker, 1998) for the dayside high-latitude ionosphere and the Hokkaido (HOK, geographic coordinates: 43.53°N, 143.61°E) radar (Nishitani et al., 2011) for the premidnight mid-latitude ionosphere.

3. Observations

3.1. Solar Wind Conditions and Geomagnetic Sudden Commencement on 16 February 2013

Figures 1a–1d show the solar wind velocity V_{sw}, the number density N_{sw}, the dynamic pressure P_{sw} ($= m_p N_{sw} V_{sw}^2$, where m_p is the mass of a proton), and the interplanetary magnetic field (IMF) magnitude B_T

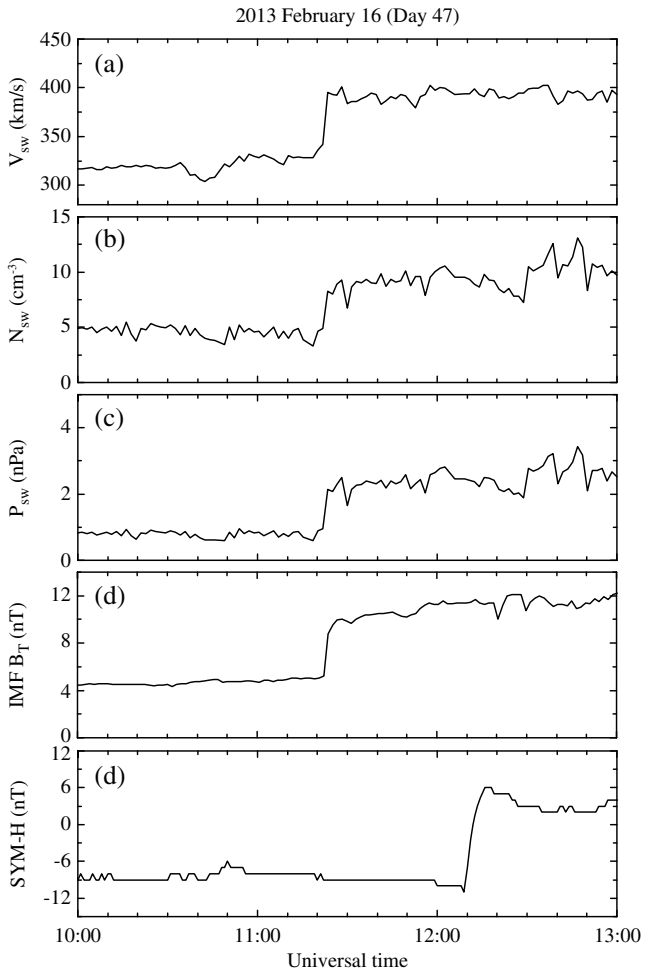

Figure 1. (a) The solar wind speed (V_{sw}), (b) solar wind density (N_{sw}), (c) the solar wind dynamic pressure (P_{sw}), (d) the magnitude of the interplanetary magnetic field (IMF B_T), and the *SYM-H* index on 16 February 2013.

for 10:00–13:00 UT on 16 February 2013. The solar wind parameters were obtained by the Wind spacecraft located near (x = 201.3, y = 76.9, z = 0.4) R_E in GSE (geocentric solar ecliptic) coordinates. The Wind spacecraft observed an interplanetary shock (i.e., sudden increases in V_{sw}, N_{sw}, P_{sw}, and the IMF B_T) around 11:20 UT.

The magnetospheric response to the interplanetary (IP) shock is clearly seen in the *SYM-H* index at ~12:09 UT about 49 min after the IP shock front passed the Wind spacecraft in the solar wind. The *SYM-H* suddenly increased about by 17 nT within 7 min. This *SYM-H* increase is classified as a sudden commencement (SC), which is caused by magnetospheric compression. That is, the middle-/low-latitude geomagnetic field change is due to the change in size of the magnetosphere, which is equivalent to changes in the magnetopause current.

3.2. SC-Associated Magnetic and Electric Field Variations in the Magnetosphere

Figure 2 shows the locations of THE-E, VAP-A, and VAP-B, projected onto the GSM x-y plane, at the onset time of the SC. The thin and thick solid curves indicate the model magnetopauses calculated by the empirical formulae of Shue et al. (1998) for IMF B_z and P_{sw} prior to and after the IP shock, respectively. We used IMF B_z = 1.8 nT and P_{sw} = 1.0 nPa for the solar wind parameters prior to the SC event, and the compressed model magnetopause was calculated with the solar wind parameters of IMF B_z = 2.0 nT and P_{sw} = 2.2 nPa. At the onset time of the SC, THE-E was around noon (MLT = 12.4) at L = ~ 6, and VAP-A and VAP-B were postmidnight (MLT = 3.2) and around midnight (MLT = 0.2), respectively, at L = ~ 5.

Figures 3a and 3b show the observed magnetic field magnitude B_T (red) along with the model B_T (blue), developed by Tsyganenko and Sitnov (2005) (TS05) at the position of THE-E, and the difference between the observed and model magnetic field magnitudes (ΔB_T). For the input parameters of the model TS05, we used the values just before the SC to exhibit the SC-associated field deviations. They were P_{sw} = 1.0 nPa, IMF B_z = 1.8 nT, IMF B_y = 4.5 nT, and Dst = −1 nT. A sudden enhancement in B_T occurred at ~12:08 UT (marked by the vertical dashed line). There was an ~1 min time delay in the SC onset times between THE-E and the Earth's surface (*SYM-H*), indicating that the initial perturbation of the SC propagated earthward with a speed of ~560 km/s. This speed is much smaller than the average equatorial Alfvén velocity of ~1,000 km/s in the dayside magnetosphere (Takahashi & Anderson, 1992). It should be noted that the time resolution of the THE-E magnetic field data is 4 s, while *SYM-H* is at 1 min resolution, having an uncertainty of ±30 s. Thus, there is difficulty in estimating the exact propagation speed of the compressional front between THE-E and the Earth's surface. ΔB_T increased to ~20 nT, which is ~15% of the unperturbed background magnetic field intensity, during the first 6 min following the SC onset and stayed at ~20 nT until 12:30 UT. This is due to the increased P_{sw} behind the shock front, as shown in Figure 1.

Figure 3c shows the y component of the electric field (E_y) measured by THE-E in geocentric solar magnetospheric (GSM) coordinates. It is clearly shown that E_y rapidly decreased by about −5 mV/m at SC onset (~12:08 UT). This negative E_y (i.e., the dusk-to-dawn electric field) perturbation beginning at magnetic field enhancement can be explained by the earthward plasma motion around noon due to the magnetospheric compression. From ~12:10 to ~12:12 UT, E_y returned to the values oscillating near zero from before the SC and then showed a small negative perturbation until 12:13 UT. Inspection of the SC-associated ΔB_T indicates that during the interval of ~12:08–12:10 UT, ΔB_T shows a rapid increase. After 12:10 UT, however, its slope becomes more gradual. This may be due to the fact that the degree of compression decreased gradually from 12:08 to 12:13 UT.

From 12:13 to 12:17 UT, E_y was positively enhanced. That is, the E_y polarity changes from negative to positive at 12:13 UT, as marked by the vertical dashed line. This SC-associated bipolar (negative-then-positive) E_y

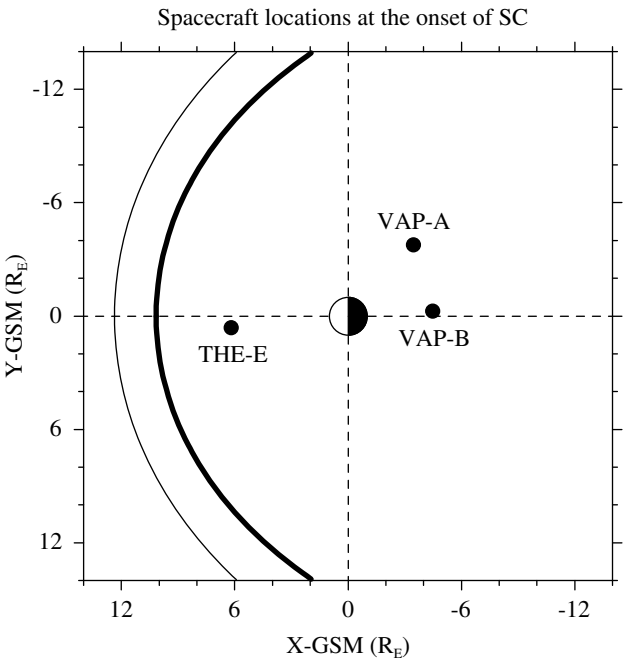

Figure 2. The three spacecraft (THE-E, VAP-A, and VAP-B) positions projected onto the geocentric solar magnetospheric *x-y* plane at the onset time of the SC. The thin solid curve indicates the model magnetopause before the SC for P_{sw} = 1.0 nPa and IMF B_z = 1.8 nT. The thick solid curve indicates the compressed model magnetopause for P_{sw} = 2.2 nPa and IMF B_z = 2.0 nT.

signature is similar to that in previous studies using the Akebono data (Shinbori et al., 2004) and THEMIS data (Kim et al., 2012). The positive E_y perturbation corresponds to sunward plasma convection. This plasma movement can be expected from a vortical plasma motion generated inside the magnetosphere as the IP shock front travels along the magnetopause (Fujita, Tanaka, Kikuchi, Fujimoto, et al., 2003; Kim et al., 2009, 2012; Yu & Ridley, 2009). After 12:17 UT, E_y is positively biased until 12:30 UT, and the average value of E_y for 12:17–12:30 UT is smaller than that for 12:13–12:17 UT. A statistical study of positively biased E_y variations after SC events has been conducted by Shinbori et al. (2006), and the authors reported that the origin of positive E_y is a plasma motion caused by compression of the magnetosphere due to the solar wind shock and discontinuity.

Figure 4 shows the magnetic field data together with the TS05 model for the parameters just before the SC and electric field data obtained by VAP-B near midnight in the inner magnetosphere ($L < 6$). The vertical dashed line indicates the SC onset time identified at THE-E around noon. Unlike the ΔB_T variations at THE-E, ΔB_T at VAP-B around midnight did not remain at an elevated level after the SC. As shown in Figure 4a, the observation agrees well with the model field before the SC. After 12:17:40 UT, however, the observed magnetic field intensity is smaller than the model field, and the deviations between the model and observation increase with time. We suggest that ΔB_T decreasing around 12:13:30 UT is due to the intensification of the cross-tail current after the SC event as the IP shock passed over the nightside magnetosphere (e.g., Park et al., 2014). The SC-associated E_y variations near midnight are plotted in Figure 4c. The bipolar (negative-then-positive) signature in E_y observed at THE-E was not identified at VAP-B. SC-associated E_y near midnight was only positively enhanced at the onset of SC, ~12:09:30 UT, and lasted until ~12:27 UT. This positive E_y perturbation is consistent with the numerical simulation by Kim et al. (2009). The authors in that study showed that the positive E_y around midnight is due to the earthward plasma flow, which is opposite to the flow direction identified around noon by THE-E, associated with the flow vortex generated near the flankside in the magnetosphere as the solar wind discontinuity passes over the magnetosphere.

Figure 5 shows the SC-associated magnetic and electric field variations observed at VAP-A in the postmidnight sector. ΔB_T suddenly increased around 12:09:09 UT, accompanied by a small decrease in E_y. This negative E_y perturbation lasted for ~1 min, which is much shorter than the negative E_y interval at THE-E around noon. The polarity of E_y changed to positive around 12:10:14 UT, and this positively enhanced E_y lasted until 12:30 UT. These E_y perturbations during the passage of the IP shock correspond to vortical plasma motions (Kim et al., 2012). The enhanced ΔB_T started to decrease around 12:13:21 UT, which can be attributed to the intensification of the SC-associated cross-tail current as mentioned above.

3.3. SuperDARN Observations

Figure 6 shows the line-of-sight (LOS) Doppler velocity maps from the Pykkvibaer (PYK) radar at 12 different times, which are selected just before the SC (Figure 6a), during the SC (Figures 6b–6h), and after the SC (Figures 6i–6l). Note that the SC interval is determined by the THE-E magnetic field data, exhibiting a steep increase in ΔB_T from 12:08 to 12:14 UT. The positive and negative velocities in Figure 6 correspond to the line-of-sight velocity toward and away from the radar, respectively, indicating an equatorward convection and a poleward convection.

At 12:07 UT before the SC (Figure 6a), the radar detected slightly positive (green) velocities at lower latitudes and strong negative (red) velocities at higher latitudes in the afternoon sector. We infer that the negative velocities representing the poleward flow (i.e., antisunward flow) at higher latitudes are driven by magnetic reconnection at the magnetopause. The positive velocities represent the return flow (i.e., sunward flow) from the magnetotail. Such a flow pattern in the field of view (FOV) of the PYK radar may be a feature resulting from a round afternoon cell driving a westward flow into the polar cap.

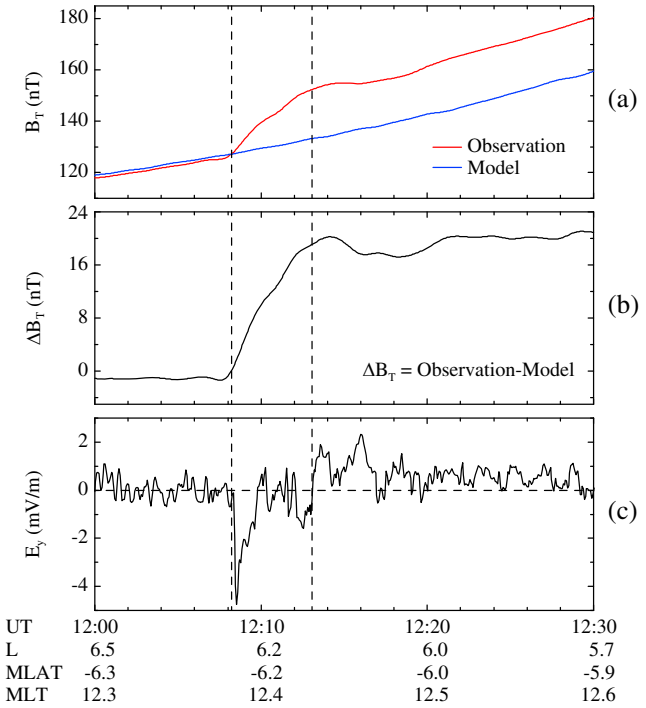

Figure 3. (a) Observed magnetic field magnitude B_T (red) at THE-E near noon and TS05 model magnetic field B_T (blue) with P_{sw} = 1.0 nPa, IMF B_z = 1.8 nT, IMF B_y = 4.5 nT, and Dst = −1 nT. (b) The difference between the observed and model magnetic field magnitudes (ΔB_T). (c) The y component of the electric field (E_y) measured by THE-E in geocentric solar magnetospheric coordinates. The vertical dashed lines at ~12:08 UT and ~12:13 UT indicate the onset of the SC and the E_y polarity change from negative to positive, respectively.

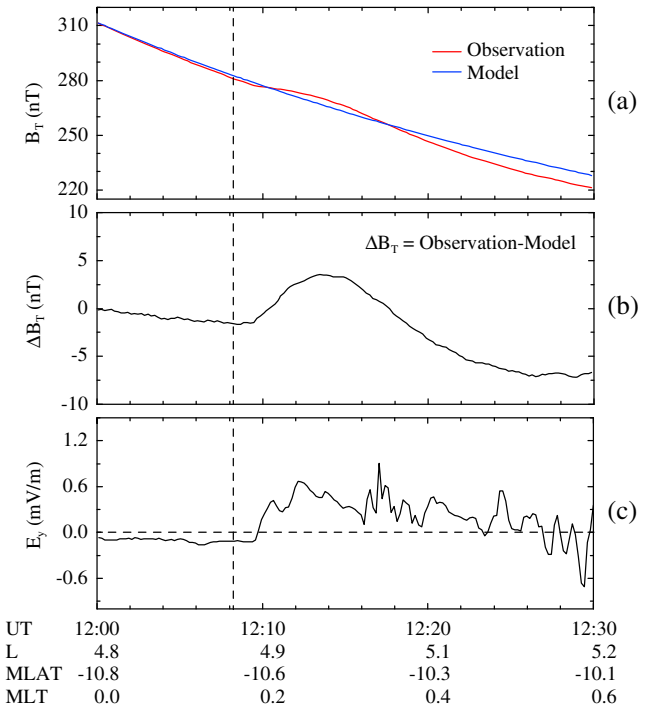

Figure 4. The format is the same as in Figure 3 except for VAP-B near midnight. The vertical dashed line indicates the onset of SC at THE-E.

Figure 6b shows the ionospheric convection at onset of the SC. There was an abrupt change in convection flows with positive velocity (equatorward convection) enhancement at 12:08 UT. This corresponds to the time of onset of the negative (dusk-to-dawn) E_y perturbation at THE-E around noon. Since the equatorward ionospheric motions at high latitudes in the dayside are due to the westward (dusk-to-dawn) electric field in the ionosphere, it is suggested that the SC-associated negative E_y observed at THE-E near noon is directly transmitted into the dayside ionosphere. The equatorward convection appears at higher latitudes (>70° MLAT) in the FOV at 12:08 UT and extended to lower latitudes (~67° MLAT), except for the southward edge of the FOV at 12:09. No dramatic equatorward motions are seen at 12:10 UT and 12:11 UT.

Negative velocity (poleward convection) was observed at 12:12 UT, and it was more enhanced after 12:14 UT. The flow reversal appears at 12:15 UT. That is, negative velocities were detected on most beams at close ranges, and positive velocities were detected in a localized region, ~14 MLT and ~75° MLAT, at further ranges. The data at 12:17 UT and 12:18 UT demonstrate that the localized positive velocities expanded toward later local times and that the negative velocities were limited toward higher latitudes with more intense velocities at further ranges. This flow reversal may be associated with the vortical plasma motion in the outer magnetosphere, which is generated near the afternoon sector as the IP shock passes over the magnetosphere (Kim et al., 2009, 2012).

In order to examine the relationship between electric field variations in the dayside outer magnetosphere and dayside ionospheric motions at high latitudes during the SC interval, we plot E_y observed at THE-E and the LOS Doppler velocity along beam 2 of the SuperDARN PYK radar and the line plot of the LOS velocity at range 27 along the beam 2, as shown in Figure 7. Two vertical dashed lines indicate the SC onset time and the time of E_y polarity change from negative to positive, respectively. Note that the PYK data are at a 1 min resolution with an uncertainty of ±30 s. To make the comparison meaningful, the E_y data resampled at 1 min intervals are plotted with blue dots in Figure 7a.

As expected from the LOS Doppler velocity maps of Figure 6, the pronounced ionospheric equatorward convection (positive velocity) was observed when E_y at THE-E was negatively enhanced, indicating that the plasma moves inward toward the satellite during magnetospheric compression. The duration of equatorward motion is comparable to that of the negative E_y perturbation. The ionospheric equatorward motions at MLAT = ~74–78° is about 30 m/s. Assuming 60,000 nT at that region, the E_y perturbation of −2 mV/m at THE-E corresponds to the ionospheric equatorward convection of ~30 m/s observed at PYK. A sudden poleward convection (negative velocity) started at 12:13 UT, when the E_y polarity changes from negative to positive, lasting until 12:18 UT. During the interval of 12:13–12:18 UT, E_y was positively enhanced. This indicates that the time-modulated ionospheric convection flows at high latitudes on the dayside are strongly correlated with the SC-associated E_y variations in the dayside magnetosphere.

After 12:18 UT, the poleward ionospheric convection turned to equatorward motion and then remained until 12:30 UT. However, there is no E_y polarity change around 12:18 UT. From 12:18 UT to 12:30 UT, as mentioned above, THE-E observed positively biased E_y variations with an average value smaller than that in the positive E_y interval of 12:13–12:18 UT.

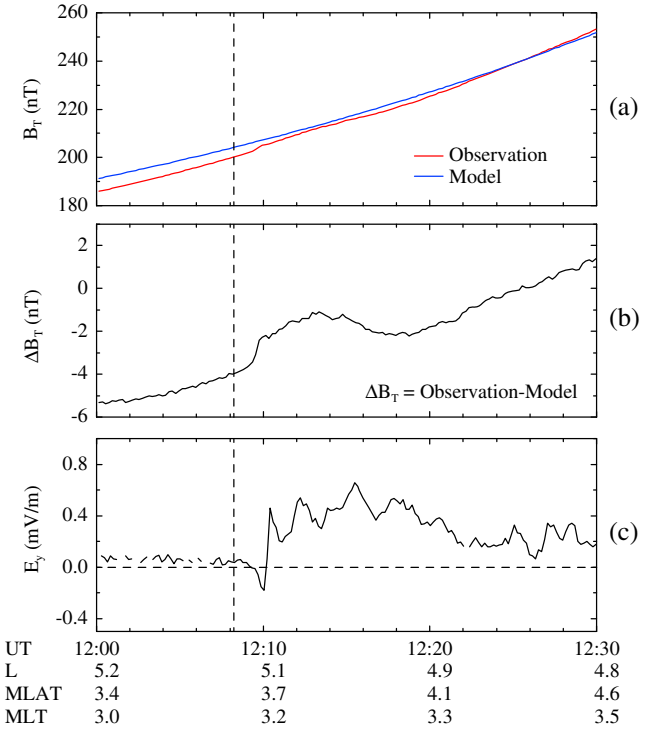

Figure 5. The format is the same as in Figure 3 except for VAP-A in the postmidnight sector. The vertical dashed line indicates the onset of SC at THE-E.

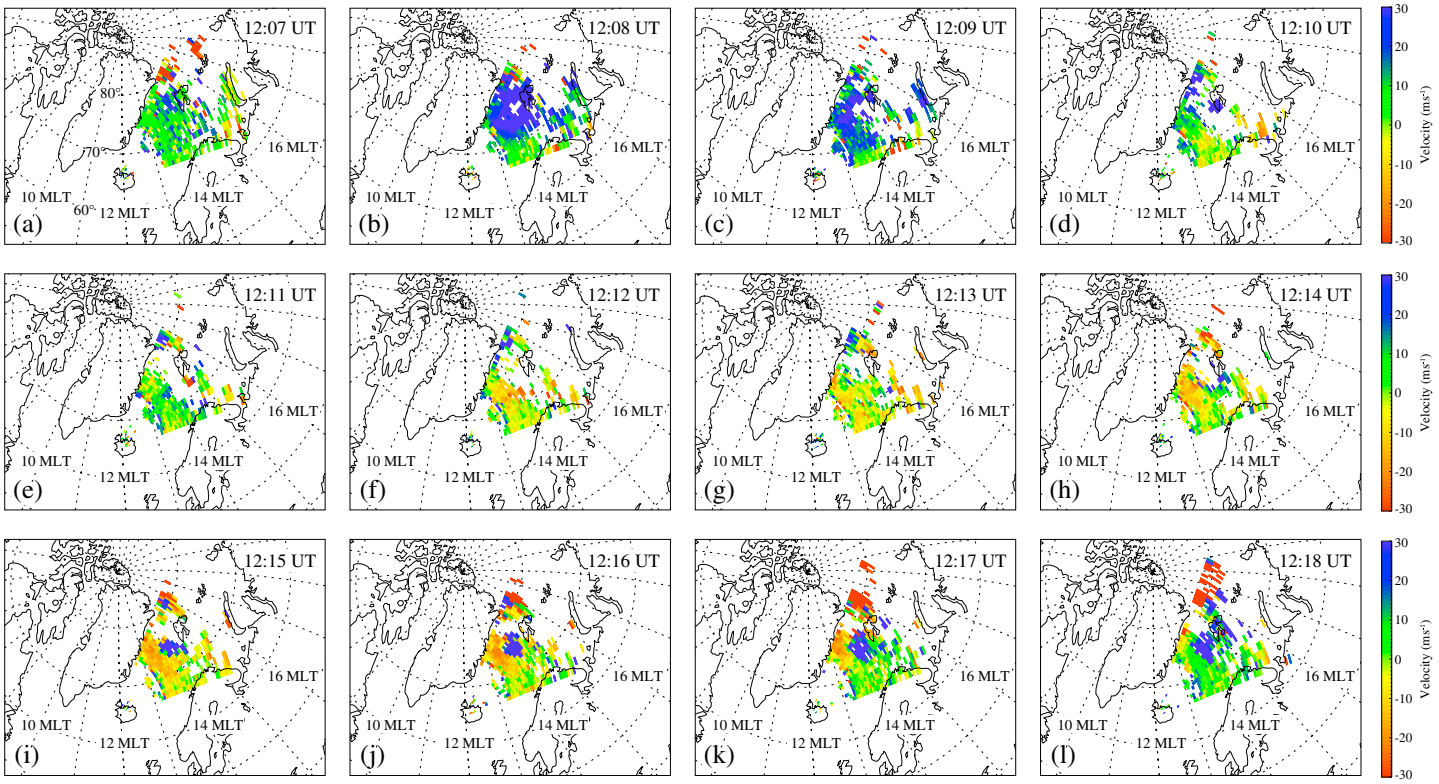

Figure 6. Line-of-sight Doppler velocity maps from the Pykkvibaer radar at 12 different times; (a) before the SC, (b–h) during the SC, and (i–l) after the SC. The positive and negative velocities correspond to the line-of-sight velocity toward and away from the radar, respectively, indicating an equatorward convection and a poleward convection.

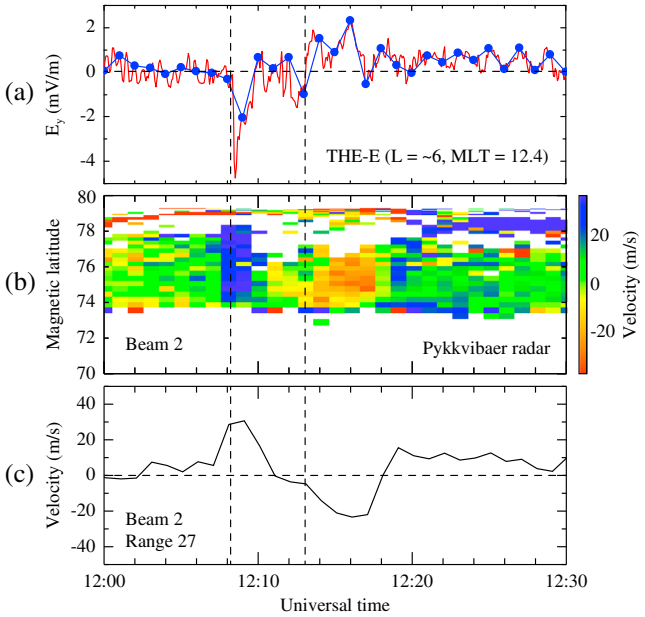

Figure 7. (a) E_y observed at THE-E. The blue dots are resampled at 1 min intervals. (b) Line-of-sight Doppler velocity along the beam 2 of the SuperDARN Pykkvibaer radar. (c) The line plot of the line-of-sight velocity at rage 27 along the beam 2. Two vertical dashed lines indicate the SC onset time and the time of E_y polarity change from negative to positive, respectively. Positive velocities are toward the radar.

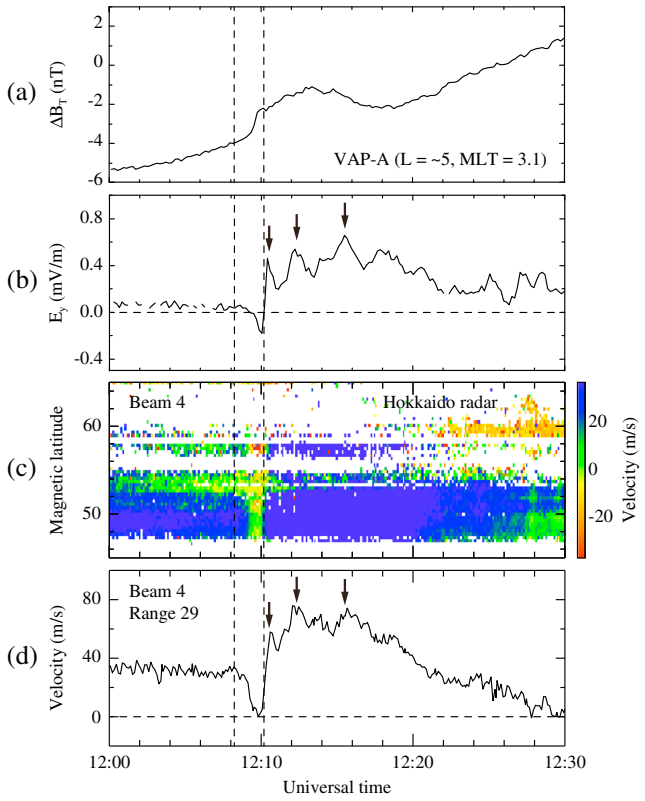

Figure 8. (a) E_y observed at VAP-A in the postmidnight sector. (b) Line-of-sight Doppler velocity along the beam 4 of the SuperDARN Hokkaido radar in the premidnight sector. (c) The line plot of the line-of-sight velocity at rage 29 along the beam 4. The vertical dashed lines at ~12:08 UT and ~12:10 UT indicate the SC onset at THE-A and E_y polarity reversal from negative to positive at VAP-A, respectively. The arrows indicate positive enhancements in E_y.

The observations of a positive E_y, corresponding to sunward plasma flow, in space at $L = \sim 5.7-6.0$ and equatorward ionospheric flow at high latitudes (>74° MLAT) can be explained in terms of the vortical plasma motion rotating counterclockwise on the afternoon side, assuming that the center of the vortex is located somewhere between the magnetopause and THE-E (i.e., $L = \sim 5.7-6.0$) and that the SuperDARN observations correspond to the plasma motion just inside the magnetopause (Kim et al., 2009; Samsonov & Sibeck, 2013; Yu & Ridley, 2009).

The SuperDARN Hokkaido (HOK) radar (Nishitani et al., 2011) measures ionospheric plasma flows at subauroral latitudes from 40° to 65° MLAT. When the IP shock hit the magnetopause and while it passed over the magnetosphere, the HOK radar was located around MLT = 21 and observed subauroral latitude ionospheric responses to the passage of the IP shock in the premidnight sector. Figures 8a–8d show the E_y values obtained by VAP-A at $L = 5.1$ in the postmidnight sector (MLT = ~3) and Doppler velocities measured by beam 4 and the line plot of the LOS velocity at range 29 (~50° geographic latitude) along beam 4 of the HOK radar in the premidnight sector. The positive (negative) values of Doppler velocities indicate horizontal motions of the ionospheric plasma irregularities toward (away from) the radar. The vertical dashed lines at ~12:08 UT and ~12:10 UT indicate the SC onset at THE-E and E_y polarity reversal from negative to positive at VAP-A, respectively. Before SC onset, the LOS Doppler velocity was positive. The velocity decreased to near zero or negative values for about 2 min after SC onset and then suddenly increased at ~12:10 UT, indicating SC-associated ionospheric motions away from the radar and then toward the radar. These ionospheric motions in the premidnight sector clearly corresponded to the SC-associated E_y variations in the postmidnight sector. That is, for a negative perturbation in E_y (i.e., a dusk-to-dawn electric field), the ionosphere responded to ionospheric motion away from the radar, and for a positive perturbation (i.e., dawn-to-dusk electric field), ionospheric motion toward the radar was measured. Furthermore, there are positive enhancements in E_y (marked by arrows) after the E_y polarity reversal. These enhancements match those in the LOS velocities of range 29 along beam 4 without a time delay. From these observations, we suggest that the electric field variations in space were the source of the ionospheric plasma motion.

3.4. High-Latitude SC Observations on the Ground

Figure 9 shows the northward (X) and eastward (Y) magnetic field components for 12:00–12:30 UT at the five high-latitude ground stations listed in Table 1 on the dayside along with the THE-E observations of E_y and ΔB. The ground stations are ordered by decreasing latitudes, from highest (Figure 9a) to lowest (Figure 9e), on the same scale. The site code, magnetic latitude, and local time at 12:10 UT are presented to the right of each panel of the ground magnetometer data. THE-E location parameters at 12:10 UT are also shown to the right. The strong negative E_y perturbation interval is marked by the vertical dashed lines at ~12:08 UT and ~12:10 UT. The vertical dashed line at 12:13 UT indicates the E_y polarity change from negative to positive.

It has been reported that the SC-associated magnetic field perturbations at high latitudes are produced by ionospheric two-cell Hall currents produced by a pair of field-aligned currents (FACs) flowing into and out of the ionosphere at latitudes of ~70° (e.g., Araki, 1994; Fujita, Tanaka, Kikuchi, Fujimoto, Hosokawa, et al., 2003; Fujita, Tanaka, Kikuchi, Fujimoto, et al., 2003; Slinker et al., 1999). At BJN, which was located at MLAT = ~71° in the afternoon sector, there was a bipolar signature (i.e., negative-then-positive perturbation) in the X component, which is consistent with the high-latitude ground magnetic field perturbations in the afternoon sector expected from the SC model developed by Araki (1994). In the Y component, however, there were no bipolar perturbations with amplitudes comparable to the X perturbation. These field signatures may be explained by the ionospheric Hall currents, first with a clockwise polarity caused by a FAC flowing into the ionosphere and then with a counterclockwise polarity caused by a FAC flowing out of the ionosphere in the afternoon sector. If BJN is located below and on the same meridian of the FAC footprints, a negative-then-positive perturbation in the X component can be expected without a significant perturbation in the Y component. Unlike at BJN, a positive-then-negative perturbation in the Y component was observed with a negative-then-positive perturbation in the X component at LYR and HOR. These X and Y perturbations imply that the both stations were located below and east of the FAC footprints. The magnitudes of the X perturbations at HOR and BJN are comparable and larger than those at the other stations located at lower and higher latitudes, indicating that the location of FAC footprints is near HOR and BJN.

For the interval of a strong negative E_y perturbation (~12:08–12:10 UT) observed at THE-E, the X components at LYR, HOR, and BJN showed positive perturbations, while negative perturbations occurred at SOR and LYC. The amplitude of the perturbation at HOR is larger than that of the other stations. This indicates that the source

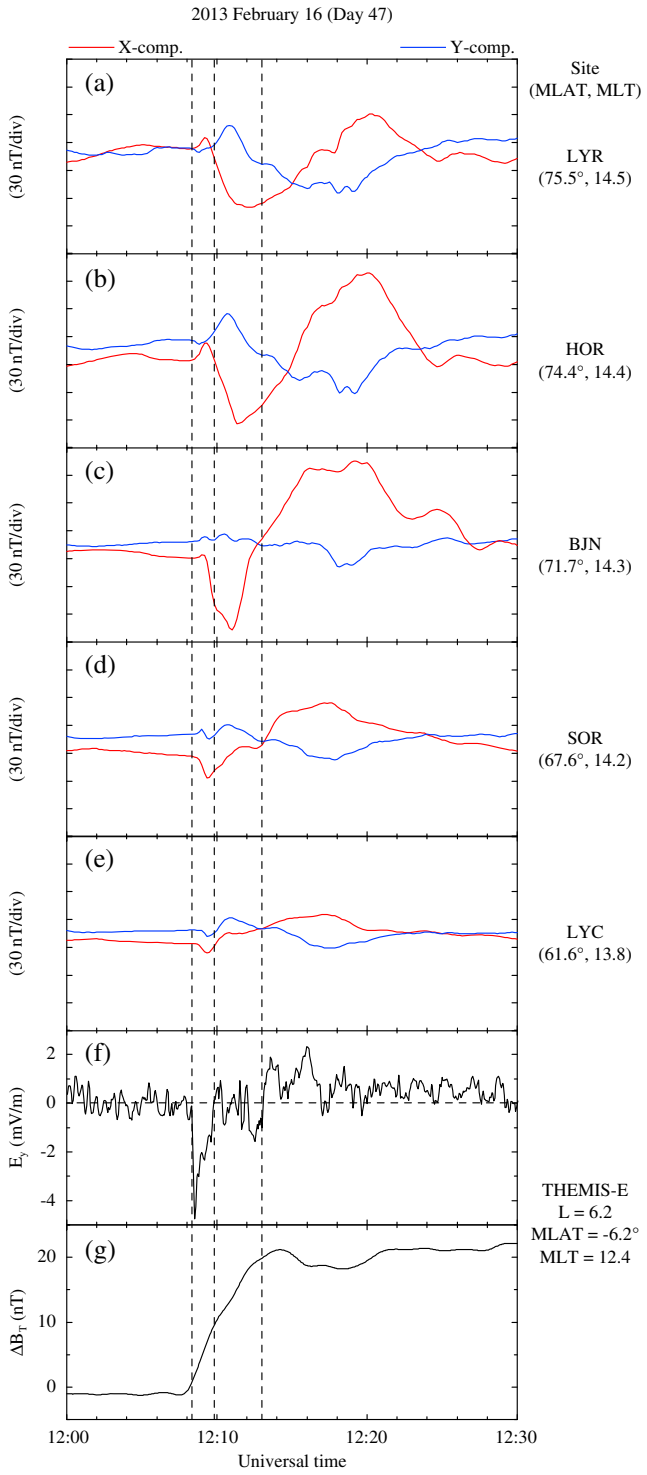

Figure 9. (a–e) The magnetic field northward (*X*) and eastward (*Y*) components for 12:00–12:30 UT at the five high-latitude ground stations selected from the IMAGE ground magnetometer network. The site code, magnetic latitude, and local time at 12:10 UT are presented to the right of each panel of IMAGE magnetometer data. (f) E_y and (g) ΔB_T observed at THE-E. The vertical dashed lines at ~12:08 UT and ~12:10 UT indicate the interval of the strong negative E_y perturbation. The vertical dashed line at 12:13 UT indicates the E_y polarity change from negative to positive.

of the perturbation is close to HOR. As mentioned above, the negative E_y perturbation in the outer magnetosphere around noon corresponds to a plasma motion toward the Earth due to magnetospheric compression. During the interval of the negative E_y perturbation, the equatorward ionospheric convection was suddenly enhanced at latitudes higher than MLAT > 70° (see Figures 6b and 6c). Thus, we suggest that the ground magnetic field perturbations preceding the large amplitude bipolar signatures are associated with magnetospheric convection in the outer magnetosphere during the initial SC interval. The X component polarity change from negative to positive at BJN appeared around 12:13 UT when the E_y polarity changed from negative to positive at THE-E. Following the vertical dashed line at 12:13 UT, we find that the positive enhancements in the X component at SOR and LYC started at that time, indicating that an SC-associated time-varying magnetospheric electric field in space is directly connected to the source of high-latitude magnetic field perturbations.

4. Discussion

We discuss the SC-associated electric field variations observed by THE-E near noon, VAP-A in the postmidnight sector, and VAP-B near midnight. During the SC interval, the negative-then-positive (i.e., dawnward-then-duskward) bipolar signature in E_y was observed at THE-E around noon (MLT = 12.4 and $L = \sim 6$). Such a bipolar E_y was also observed at VAP-A in the postmidnight sector (MLT = ~ 3.2 and $L = \sim 5$) with a short duration time for the negative E_y perturbation. These bipolar E_y signatures in our study are similar to previous observations by the THEMIS probes in the prenoon sector (Kim et al., 2012) and by the Akebono satellite in the dawnside inner magnetosphere (Shinbori et al., 2004). Near the midnight sector (MLT = 0.3 and $L = \sim 5$), however, VAP-B observed only a positive (duskward) E_y deflection without a negative E_y perturbation. This indicates that the E_y signatures are more complicated than the SC-associated magnetic field variations in space.

The behavior of the SC-associated initial E_y disturbances around noon and midnight is puzzling when trying to fit our observations with the Araki's SC model. In the SC model the PI signature results from a compressional impulse launched at the dayside magnetopause where an IP shock hit. Such a compressional magnetospheric disturbance propagates tailward as a fast mode wave (e.g., Keika et al., 2009; Wilken et al., 1982). THE-E around noon observed a sudden dawnward enhancement in E_y. If this E_y signature is associated with a fast mode wave, the Poynting vector of the initial SC impulse is directed tailward because of dawnward E_y perturbation (negative δE_y) and northward B_z perturbation (positive δB_z). If the initial magnetic field perturbation (i.e., a positive δB_z) observed at VAP-B around midnight is caused by a fast mode wave propagating tailward, a dawnward E_y perturbation must be detected near midnight because the electromagnetic energy of the compressional pulse is directed tailward. However, the observations at VAP-B around midnight indicate earthward Poynting flux because the initial E_y perturbation is duskward. This is not a unique case. In a statistical study of SC-related electric field perturbations by Shinbori et al. (2004), the authors reported that there is no Poynting vector for the initial SC impulse directed tailward in the nightside sector. Thus, it is questionable whether the PI signature shown at BJN for the interval of ~12:08–12:13 UT is associated with a fast mode wave.

Previous ground observations have reported that the footprints of PI-associated FACs in the ionosphere are located around the magnetic latitudes of ~70°–75° (e.g., Araki, 1994; Engebretson et al., 1999; Moretto et al., 2000). This location corresponds to a radial distance of $L > 8$ in the magnetosphere. In Araki's SC model, the PI-associated FACs are converted via coupling of the compressional signal launched at the magnetopause by a sudden compression. This mode conversion from the compressional mode to the Alfvén mode occurs most effectively in a region of a steep Alfvén speed gradient (e.g., Lee at al., 2004; Tamao, 1965). Such a region has not been reported in the outer magnetosphere ($L > 8$) but instead near the plasmapause (Takahashi & Anderson, 1992). Fujita, Tanaka, Kikuchi, Fujimoto, Hosokawa, et al. (2003) showed that the PI-FACs appear around a 70° magnetic latitude, resulting in the mode coupling from fast mode waves to Alfvén waves. However, they did not used a realistic Alfvén speed profile for the magnetosphere in their numerical study.

In a numerical simulation of SC that assumed a monotonic radial Alfvén speed profile without including a plasmasphere model (Yu & Ridley, 2009), the inductive electric field, which is caused by the fast mode wave, generates a dusk-to-dawn displacement current just inside the dayside magnetopause for the PI phase, and the displacement current turns to FACs flowing into the ionosphere on the afternoon side and out of the ionosphere on the morning side at around 73° MLAT. Note that the region mapped into the magnetosphere is not near a significant Alfvén speed gradient. Yu and Ridley (2009) suggested that the change in the current

path from the displace current to the FAC may be associated with the enhanced cusp dynamics that result from fast mode propagation toward the cusp region. Thus, it is possible to produce PI-FACs without invoking the mode conversion.

The SC results from a significant compression of the magnetosphere for several minutes. This indicates that the initial negative E_y perturbation observed at THE-E around noon corresponds to the earthward plasma motion caused by the inward movement of the dayside magnetopause. That is, the electric field is related to the dynamic motion of the dayside magnetopause. Comparing E_y at THE and the SuperDARN PYK radar data, we confirmed that the strongly enhanced equatorward ionospheric convection appeared for the interval, 12:08–12:10 UT, of the strong negative E_y perturbation. From these observations we suggest that the magnetospheric flows are strongly connected to the ionospheric flows during the SC interval. The equatorward ionospheric convection is latitudinally limited to ~70° from higher latitudes, as shown in Figure 6c. This can be explained by the deceleration of the earthward magnetospheric plasma motion. Since the background magnetic field strength increases as the plasma moves earthward, the inertia current flowing from the morning to the afternoon can be generated due to the deceleration of plasma flows. The electric field direction is opposite to the inertia current direction. Thus, the current is the dynamo current. If the inertia current is converged in the afternoon and diverged in the morning (Fujita, Tanaka, Kikuchi, Fujimoto, et al., 2003), then the polarity of FACs is the same as that of PI-associated FACs in the SC model. If the ground magnetic field perturbations, plotted in Figure 9, for ~12:08–12:10 UT are produced by the clockwise Hall current induced by a FAC flowing into the ionosphere, the center of the Hall current is located somewhere between HOR and SOR. Thus, it should be numerically examined whether the electric field variations for the PI phase are associated with fast mode waves or magnetospheric convection responding to the solar wind dynamic pressure variations.

Kim et al. (2009) numerically investigated the convective electric fields during the SC interval for various local times at $L = 4.65$ (see Figure 4 in their study) and clearly showed a negative-then-positive (i.e., bipolar) perturbation in E_y around noon. Along the local time from noon to the premidnight sector, the duration of negative E_y perturbation becomes shorter, and it disappears around midnight. These SC-associated E_y variations in the numerical study, which are very consistent with our observations, have been attributed to vortical plasma motions rotating counterclockwise in the afternoon sector. Since magnetic field lines in the outer magnetosphere are frozen in the rotating flows and are anchored at high latitudes, the rotating magnetospheric flux tube is twisted in a sense of a clockwise rotation in the ionosphere, leading to an upward FAC. As shown in Figures 6i–6k, we confirmed a clockwise rotation of the ionospheric flows at high latitudes (>70° MLAT) for the interval of positive E_y. Thus, a large perturbation in the X-component at HOR and BJN in the MI phase is due to the counterclockwise ionospheric Hall current caused by the upward FAC in the afternoon, as mentioned above.

5. Conclusion

We examined the properties of SC-associated electric field variations observed simultaneously near noon, postmidnight, and midnight in the magnetosphere. The overall appearance of the SC-associated electric field differs considerably at different local times. Around noon at L =~6, a dawnward-then-duskward electric field perturbation was observed. Such a two-phase structure of the SC-associated electric field perturbation is related to the ground SC perturbation at high latitudes. That is, the dawnward electric field perturbation corresponds to the PI phase and the duskward perturbation corresponds to the MI phase. In the postmidnight sector at L =~5, the amplitude and duration time of the dawnward electric field perturbation is weaker and shorter than that around noon. Near midnight at L =~5, there were no occurrences of dawnward electric field perturbation. If the dawnward electric field perturbation is associated with a fast mode compressional wave launched at the dayside magnetopause by an IP shock, the fast mode wave greatly weakens as it propagates tailward. Using the SuperDARN radar data, we confirmed that the ionospheric plasma motions during the SC are mainly due to the electric field variations observed in space. This indicates that the SC-associated electric field in space plays a significant role in determining the dynamic variations of the ionospheric convection flow. It should be noted that the present study is based on only one SC event. Obviously, quantitative and qualitative arguments presented above cannot be generalized. In the future, we need a large data set of SC events observed in the magnetosphere and ionosphere to understand the magnetospheric and ionospheric responses to solar wind dynamic pressure variations. It will be interesting to study the difference in the effects on convection flows associated with slow varying SC and fast varying SC.

Acknowledgments
The solar wind data are available at the NASA OMNIWeb service (http://omniweb.gsfc.nasa.gov/). The THEMIS data used in this study were obtained from the THEMIS website (http://themis.ssl.berkeley.edu). The Van Allen Probe data were obtained from the coordinated data analysis web (http://cdaweb.gsfc.nasa.gov/cdaweb). The authors thank the institutes who maintain the IMAGE Magnetometer Array. IMAGE data are available at http://www.space.fmi.fi/image/. The *SYM-H* index is provided through WDC-C2 for Geomagnetism, Kyoto University (http://wdc.kugi.kyoto-u.ac.jp). The authors acknowledge the use of SuperDARN data. SuperDARN is a collection of radars funded by national scientific funding agencies of Australia, Canada, China, France, Japan, South Africa, United Kingdom, and United States of America. We thank the EMFISIS team for providing wave data from the Van Allen Probe spacecraft which was supported by JHU/APL contract 921647 under NASA Prime contract NAS5-01072 and JHU/APL contract 131802 under NASA prime contract NNN06AA01C. This work was supported by BK21+ through the National Research Foundation (NRF) funded by the Ministry of Education of Korea. The work of K.-H. Kim was supported by the Basic Science Research Program through NRF funded by NRF-2016R1A2B4011553 and also supported by project PE17020 of the Korea Polar Research Institute.

References

Araki, T. (1994). A physical model of the geomagnetic sudden commencement. In M. J. Engebretson, K. Takahashi, & M. Scholer (Eds.), *Solar wind sources of magnetospheric ultra-low-frequency waves, Geophysical Monograph Series* (Vol. 81, pp. 183), Washington, DC: American Geophysical Union.

Auster, H. U., Glassmeier, K. H., Magnes, W., Aydogar, O., Baumjohann, W., Constantinescu, D., … Wiedemann, M. (2008). The THEMIS fluxgate magnetometer. *Space Science Reviews*, *141*, 235–263. https://doi.org/10.1007/s11214-008-9365-9

Baumjohann, W., Bauer, O. H., Haerendel, G., & Junginger, H. (1983). Magnetospheric plasma drifts during a sudden impulse. *Journal of Geophysical Research*, *88*, 9287–9289.

Bonnell, J. W., Mozer, F. S., Delory, G. T., Hull, A. J., Ergun, R. E., Cully, C. M., … Harvey, P. R. (2008). The Electric Field Instrument (EFI) for THEMIS. *Space Science Reviews*, *141*, 303–341. https://doi.org/10.1007/s11214-008-9469-2

Borodkova, N., Zastenker, G., Riazantseva, M., & Richardson, J. (2005). Large and sharp solar wind dynamic pressure variations as a source of geomagnetic field disturbances at the geosynchronous orbit. *Planetary and Space Science*, *53*, 25–32.

Chen, L., & Hasegawa, A. (1974). A theory of long-period magnetic pulsations: 2. Impulse excitation of surface eigenmode. *Journal of Geophysical Research*, *79*, 1033–1037.

Engebretson, M. J., Murr, D. L., Hughes, W. J., Lühr, H., Moretto, T., Posch, J. L., … Bitterly, M. (1999). A multipoint determination of the propagation velocity of a sudden commencement across the polar ionosphere. *Journal of Geophysical Research*, *104*(A10), 22,433–22,451.

Fujita, S., Tanaka, T., Kikuchi, T., Fujimoto, K., Hosokawa, K., & Itonaga, M. (2003). A numerical simulation of the geomagnetic sudden commencement: 1. Generation of the field-aligned current associated with the preliminary impulse. *Journal of Geophysical Research*, *108*, 1416. https://doi.org/10.1029/2002JA009407

Fujita, S., Tanaka, T., Kikuchi, T., Fujimoto, K., & Itonaga, M. (2003). A numerical simulation of the geomagnetic sudden commencement: 2. Plasma processes in the main impulse. *Journal of Geophysical Research*, *108*, 1417. https://doi.org/10.1029/2002JA009763

Huttunen, K. E. J., Slavin, J., Collier, M., Koskinen, H. E. J., Szabo, A., Tanskanen, E., … Reme, H. (2005). Cluster observations of sudden impulses in the magnetotail caused by interplanetary shocks and pressure increases. *Annales de Geophysique*, *23*, 609–624.

Iyemori, T., & Rao, D. R. (1996). Decay of the *Dst* field of geomagnetic disturbance after substorm onset and its implication to storm-substorm relation. *Annales de Geophysique*, *14*, 608–618. https://doi.org/10.1007/s00585-996-0608-3

Kawano, H., Yamamoto, T., & Kokubun, S. (1992). Rotational polarities of sudden impulses in the magnetotail lobe. *Journal of Geophysical Research*, *97*, 17,177–17,182.

Keika, K., Nakamura, R., Baumjohann, W., Angelopoulos, V., Chi, P. J., Glassmeier, K. H., … Dandouras, I. (2009). Substorm expansion triggered by a sudden impulse front propagating from the dayside magnetopause. *Journal of Geophysical Research*, *114*, A00C24. https://doi.org/10.1029/2008JA013445

Kim, K.-H., Cattell, C. A., Lee, D.-H., Takahashi, K., Yumoto, K., Shiokawa, K., … Andre, M. (2002). Magnetospheric responses to sudden and quasiperiodic solar wind variations. *Journal of Geophysical Research*, *107*(A11), 1406. https://doi.org/10.1029/2002JA009342

Kim, K.-H., Cattell, C. A., Lee, D.-H., Balogh, A., Lucek, E., Andre, M., … Reme, H. (2004). Cluster observations in the magnetotail during sudden and quasiperiodic solar wind variations. *Journal of Geophysical Research*, *109*, A04219. https://doi.org/10.1029/2003JA010328

Kim, K.-H., Lee, D.-H., Shiokawa, K., Lee, E., Park, J.-S., Kwon, H.-J., … Baishev, D. G. (2012). Magnetospheric responses to the passage of the interplanetary shock on 24 November 2008. *Journal of Geophysical Research*, *117*, A10209. https://doi.org/10.1029/2012JA017871

Kim, K.-H., Park, K. S., Ogino, T., Lee, D.-H., Sung, S.-K., & Kwak, Y.-S. (2009). Global MHD simulation of the geomagnetic sudden commencement on 21 October 1999. *Journal of Geophysical Research*, *114*, A08212. https://doi.org/10.1029/2009JA014109

Kletzing, C., Kurth, W. S., Acuna, M., MacDowall, R. J., Torbert, R. B., Averkamp, T., … Tyler, J. (2013). The Electric and Magnetic Field Instrument Suite and Integrated Science (EMFISIS) on RBSP. *Space Science Reviews*, *179*, 127–181. https://doi.org/10.1007/s11214-013-9993-6

Knott, K. J., Pedersen, A., & Wedersen, U. (1985). GEOS 2 electric field observations during a sudden commencement and subsequent substorms. *Journal of Geophysical Research*, *90*, 1283–1288.

Kokubun, S. (1983). Characteristics of storm sudden commencement at geostationary orbit. *Journal of Geophysical Research*, *88*, 10,025–10,033.

Kuwashima, M., Tsunomura, S., & Fukunishi, H. (1985). SSC-associated magnetic variations at the geosynchronous altitude. *Journal of Atmospheric and Solar-Terrestrial Physics*, *47*, 451–461.

Lee, D.-H., Lysak, R. L., & Song, Y. (2004). Investigations of MHD wave coupling in a 3-D numerical model: Effects of temperature gradients. *Advances in Space Research*, *33*, 742–746.

Lepping, R. P., Acũna, M. H., Burlaga, L. F., Farrell, W. M., Slavin, J. A., Schatten, K. H., … Worley, E. M. (1995). The wind magnetic field investigation. *Space Science Reviews*, *71*, 207–229.

Lühr, H. (1994). The IMAGE magnetometer network. *STEP International Newsletter*, *4*, 4–6.

Moretto, T, Ridley, A. J., Engebretson, M. J., & Rasmussen, O. (2000). High-latitude ionospheric response to a sudden impulse event during northward IMF conditions. *Journal of Geophysical Research*, *105*(A2), 2521–2531.

Nishitani, N., Ogawa, T., Otsuka, Y., Hosokawa, K., & Hori, T. (2011). Propagation of large amplitude ionospheric disturbances with velocity dispersion observed by the SuperDARN Hokkaido radar after the 2011 off the Pacific coast of Tohoku earthquake. *Earth, Planets and Space*, *63*, 891–896. https://doi.org/10.5047/eps.2011.07.003

Nopper, R. W., Hughes, W. J., Maclennan, C. G., & McPherron, R. L. (1982). Impulse-excited pulsations during the July 29, 1977, event. *Journal of Geophysical Research*, *87*, 5911–5916.

Ogilvie, K. W., Chornay, D. J., Fritzenreiter, R. J., Hunsaker F., Keller, J., Lobell, J., … Gergin, E. (1995). SWE, a comprehensive plasma instrument for the WIND spacecraft. *Space Science Reviews*, *71*, 55–77.

Park, J.-S., Kim, K.-H., Kwon, H.-J., Lee, E., Lee, D.-H., Jin, H., & Hwang, J. (2014). Statistical analysis of geosynchronous magnetic field perturbations near midnight during sudden commencements. *Journal of Geophysical Research*, *119*, 4668–4680. https://doi.org/10.1002/2013JA019380

Park, J.-S., Kim, K.-H., Lee, D.-H., Araki, T., Lee, E., & Jin, H. (2012). Statistical analysis of SC-associated geosynchronous magnetic field perturbations. *Journal of Geophysical Research*, *117*, A09212. https://doi.org/10.1029/2012JA017648

Ruohoniemi, J. M., & Baker, K. B. (1998). Large-scale imaging of the high-latitude convection with Super Dual Auroral Radar Network HF radar observations. *Journal of Geophysical Research*, *103*(A9), 20,797–20,811. https://doi.org/10.1029/98JA01288

Russell, C. T., Ginskey, M., Petrinec, S., & Le, G. (1992). The effect of solar wind dynamic pressure changes on low and mid-latitude magnetic records. *Geophysical Research Letters*, *19*, 1227–1230.

Samsonov, A. A., & Sibeck, D. G. (2013). Large-scale flow vortices following a magnetospheric sudden impulse. *Journal of Geophysical Research: Space Physics*, *118*, 3055–3064. https://doi.org/10.1002/jgra.50329

Samsonov, A. A., Sibeck, D. G., & Yu, Y.-Q. (2010). Transient changes in magnetospheric-ionospheric currents caused by the passage of an interplanetary shock: Northward interplanetary magnetic field case. *Journal of Geophysical Research*, *115*, A05207. https://doi.org/10.1029/2009JA014751

Shepherd, S. G. (2014). Altitude-adjusted corrected geomagnetic coordinates: Definition and functional approximations. *Journal of Geophysical Research: Space Physics*, *119*, 7501–7521. https://doi.org/10.1002/2014JA020264

Shi, Q. Q., Hartinger, M. D., Angelopoulos, V., Tian, A. M., Fu, S. Y., Zong, Q.-G., … Shen, X. C. (2014). Solar wind pressure pulse-driven magnetospheric vortices and their global consequences. *Journal of Geophysical Research: Space Physics*, *119*, 4274–4280. https://doi.org/10.1002/2013JA019551

Shinbori, A., Ono, T., Iizima, M., & Kumamoto, A. (2004). SC related electric and magnetic field phenomena observed by the Akebono satellite inside the plasmasphere. *Earth, Planets and Space*, *56*, 269–282.

Shinbori, A., Ono, T., Iizima, M., Kumamoto, A., & Nishimura, Y. (2006). Enhancements of magnetospheric convection electric field associated with sudden commencements in the inner magnetosphere and plasmasphere regions. *Advances in Space Research*, *38*, 1595–1607.

Shue, J.-H., Song, P., Russell, C. T., Steinberg, J. T., Chao, J. K., Zastenker, G., … Kawano, H. (1998). Magnetopause location under extreme solar wind conditions. *Journal of Geophysical Research*, *103*(A8), 17,691–17,700.

Slinker, S. P., Fedder, J. A., Hughes, W. J., & Lyon, J. G. (1999). Response of the ionosphere to a density pulse in the solar wind: Simulation of travelling convection vortices. *Geophysical Research Letters*, *26*, 3549–3552.

Southwood, D. J. (1974). Some features of field line resonances in the magnetosphere. *Planetary and Space Science*, *22*, 483–491.

Sugiura, M., Skillman, T. L., Ledley, B. G., & Heppner, J. P. (1968). Propagation of the sudden commencement of July 8, 1966, to the magnetotail. *Journal of Geophysical Research*, *73*, 6699–6709.

Sun, T. R., Wang, C., Zhang, J. J., Pilipenko, V. A., Wang, Y., & Wang, J. Y. (2015). The chain response of the magnetospheric and ground magnetic field to interplanetary shocks. *Journal of Geophysical Research: Space Physics*, *120*, 157–165. https://doi.org/10.1002/2014JA020754

Takahashi, K., & Anderson, B. J. (1992). Distribution of ULF energy ($f < 80$ mHz) in the inner magnetosphere: A statistical analysis of AMPTE CCE magnetic field data. *Journal of Geophysical Research*, *97*, 10,751–10,773.

Tamao, T. (1965). Transmission and coupling resonance of hydromagnetic disturbances in the non-uniform Earth's magnetosphere. *Science Reports of the Tohoku University: Geophysics*, *17*, 43–72.

Tian, A. M., Shen, X. C., Shi, Q. Q., Tang, B. B., Nowada, M., Zong, Q. G., & Fu, S. Y. (2016). Dayside magnetospheric and ionospheric responses to solar wind pressure increase: Multispacecraft and ground observations. *Journal of Geophysical Research: Space Physics*, *121*, 10,813–10,830. https://doi.org/10.1002/2016JA022459

Tsyganenko, N. A., & Sitnov, M. I. (2005). Modeling the dynamics of the inner magnetosphere during strong geomagnetic storms. *Journal of Geophysical Research*, *110*, A03208. https://doi.org/10.1029/2004JA010798

Villante, U., & Piersanti, M. (2008). An analysis of sudden impulses at geosynchronous orbit. *Journal of Geophysical Research*, *113*, A08213. https://doi.org/10.1029/2008JA013028

Wang, C., Liu, J. B., Li, H., Huang, Z. H., Richardson, J. D., & Kan, J. R. (2009). Geospace magnetic field responses to interplanetary shocks. *Journal of Geophysical Research*, *114*, A05211. https://doi.org/10.1029/2008JA013794

Wilken, B., Goertz, C. K., Baker, D. N., Higbie, P. R., & Fritz, T. A. (1982). The SSC on July 29, 1977 and its propagation within the magnetosphere. *Journal of Geophysical Research*, *87*, 5901–5910.

Wygant, J. R., Bonnell, J. W., Goetz, K., Ergun, R. E., Mozer, F. S., Bale, S. D., … Tao, J. B. (2013). The Electric Field and Waves (EFW) instruments on the Radiation Belt Storm Probes Mission. *Space Science Reviews*, *179*, 183–220. https://doi.org/10.1007/s1124-013-0013-7

Yu, Y., & Ridley, A. J. (2009). The response of the magnetosphere-ionosphere system to a sudden dynamic pressure enhancement under southward IMF conditions. *Annales de Geophysique*, *27*, 4391–4407.